HiSST: 3rd International Conference on
High-Speed Vehicle Science Technology
14 -19 April 2024, Busan, Korea

Transient Analysis of the Conjugate Heat Transfer Analysis of High-Speed Vehicle Engine Inlet

Jae-Eun Kim[1], Jeong-Yeol Choi[2]

Abstract

A conjugate heat transfer analysis was conducted for the High-speed vehicle inlet. We examined the internal flow and the structure temperature variations over time. In the time frame of less than 10 seconds, noticeable differences in the internal flow were observed along with rapid heat conduction. However, after 10 seconds, apart from the solid temperature on the upper wall, there were no noticeable differences in the internal flow patterns. In the constant wall temperature condition, the solid domains temperature increased similarly to the adiabatic condition, but the wall temperature was not heated above a certain level.

Keywords: *High-speed vehicle, Conjugate heat transfer*

Nomenclature

Q – Conservative variable vector
F, Q – Convective flux vector
F_v, Q_v – Viscous flux vector
F_s, Q_s – Flux vector for solid

Greek
θ – Nondimensionalized temperature
Subscripts
i – Initial
∞ – Freestream

1. Introduction

High-speed vehicle performs powered flight for tens to hundreds of seconds. As an example for a high-speed airplane, the operating conditions of the HyShot model for ground test were set to a flight Mach number of 5-6 at an altitude of 20 km. Previous studies using DES to analyze combustion set the Mach number of the inlet flow to 3 and the temperature to 600 K. A complex temperature field ranging from 200 K to 3,000 K is distributed before and after the injector [1-4]. Another high-speed vehicle geometry uses air-throttling of the expansion part to block the flow at subsonic speeds to ignition. A few milliseconds later, the fuel and air mix and ignition occurs, creating a temperature field of up to 2,000 K [5-7]. A number of previous studies presented the high temperature flow field inside the scramjet combustor [8-14].
To create a high–speed environment on the ground test, a test vehicle directly connected to vitiated air heater(VAH) or a high–speed wind tunnel is used. When testing in a VAH, the aircraft structure is heated to a high temperature as a high enthalpy flow is supplied, and when testing in a high–speed wind tunnel, the internal and external surfaces are also heated by the high–speed wind tunnel flow.[15-19] There is a risk that such a heated structure will change the internal flow field of the aircraft, resulting in performance that is different from the initial design point. Therefore, in this study, a conjugate heat transfer analysis was conducted to investigate of temperature variations over time on the various boundary conditions.

[1] *Doctoral Student, Department of Aerospace Engineering, Pusan National University, aerokje2@pusan.ac.kr*
[2] *Professor, Department of Aerospace Engineering, Pusan National University, aerochoi@pusan.ac.kr*

2. Numerical Methodology

2.1. Governing Equation

In the present study RPL2D, in-house code is used, which has been developed at the Rocket Propulsion Laboratory of Pusan National University and used for the validation and application problems for a long time [20-36]. This program involves solving a set of governing equations that encompass species conservation, the Navier–Stokes equation, and energy conservation. The turbulence model is Menter's two–equation k–ω SST model [37]. The turbulence model has been studied for scramjet flow field with various conditions [38-43].The governing equations are structured in a conservative vector form and discretized using the finite–volume method.

In the fluid simulation, the convective flux term in the governing equations is discretized using the RoeM scheme, which is combined with the MUSCL scheme to achieve high–order spatial accuracy. To preserve the Total Variation Diminishing (TVD) property, the β–minmod limiter [44] is employed. For the viscous flux term, a second–order accurate central difference scheme is utilized. The time integration is carried out using LU–SGS [45]. Further details of the mathematical modeling and numerical methods are described in the literatures [1-43].

$$\frac{\partial Q}{\partial t}+\frac{\partial F}{\partial x}+\frac{\partial G}{\partial y}=\frac{\partial F_v}{\partial x}+\frac{\partial G_v}{\partial y} \tag{1}$$

$$Q=\begin{bmatrix}\rho_k\\ \rho u\\ \rho v\\ e\\ \rho k\\ \rho\omega\end{bmatrix}, F=\begin{bmatrix}\rho_k u\\ \rho u^2+p\\ \rho uv\\ (e+p)u\\ \rho uk\\ \rho u\omega\end{bmatrix}, G=\begin{bmatrix}\rho_k v\\ \rho uv\\ \rho v^2+p\\ (e+p)v\\ \rho vk\\ \rho v\omega\end{bmatrix}, F_v=\begin{bmatrix}-\rho_k u_k^d\\ \tau_{xx}\\ \tau_{xy}\\ \beta_x\\ \mu_k\,\partial k/\partial x\\ \mu_\omega\,\partial\omega/\partial x\end{bmatrix}, G_v=\begin{bmatrix}-\rho_k u_k^d\\ \tau_{xy}\\ \tau_{yy}\\ \beta_y\\ \mu_k\,\partial k/\partial y\\ \mu_\omega\,\partial\omega/\partial y\end{bmatrix} \tag{2}$$

For CHT analysis, RPL2D is modified. A dimensionless energy equation is incorporated into the RPL2D. The spatial term of this energy equation is discretized using a second–order central difference scheme, while the time term is discretized using a first–order forward difference scheme.

We selected loosely coupled strategy because of the short time scale. The surface temperature of the solid domain is provided to the fluid domain as a Dirichlet boundary condition. Once the fluid domain calculations are completed, the wall heat flux is then transferred to the solid domain as a Neumann boundary condition. This iterative process continues until the desired time is reached. The validation of the CHT solver is carried out through a cylindrical leading–edge model that underwent testing in the NASA Langley 8 ft wind tunnel [46-47]. More details about the CHT solver are described in the previous study [48].

$$\frac{\partial Q}{\partial t}=\frac{\partial F_s}{\partial x}+\frac{\partial G_s}{\partial y} \tag{3}$$

$$Q=\theta\equiv\frac{T-T_w}{T_w}, F_s=\frac{\partial\theta}{\partial x}, G_s=\frac{\partial\theta}{\partial y} \tag{4}$$

2.2. Numerical domains and boundary conditions

The adiabatic assumption is applied to the lip tip and double wedge due to the tip being subjected to stagnation temperature and subsystems like batteries being mounted on the wedges. Therefore, the insulated area grids for the solid walls are excluded from the simulation. Thickness of the solid wall is approximately 7.5 mm. We assumed that the vehicle is made by Inconel 625. The physical and thermal properties are shown in Table 1.

The High-speed vehicle engine inlet operates at Mach 6.4, Reynold's number 1.7×10^7. In Figure 1, fluid domains have the left side set as the inflow boundary condition, the right side as the outflow boundary condition, and the bottom side as the far–field boundary condition. Except that, all the surface is set as the no–slip wall boundary condition. Constant temperature was given to the external walls and the results for different temperature conditions were compared. For the adiabatic condition, the interior walls were given an insulated condition, assuming that the walls of the flow path are covered with

insulation. We refer to the insulation condition as Adiabatic and the constant temperature wall as CnsT (set temperature) K. The number of the total grid point is 118,235. The initial temperature of solid domains is 300 K.

Table 1. Physical and thermal properties of Inconel 625

Physical and thermal properties	Values
Mass density, kg/m^3	8,440
Specific heat capacity, J/kg·K	410
Thermal conductivity, W/m·K	9.8

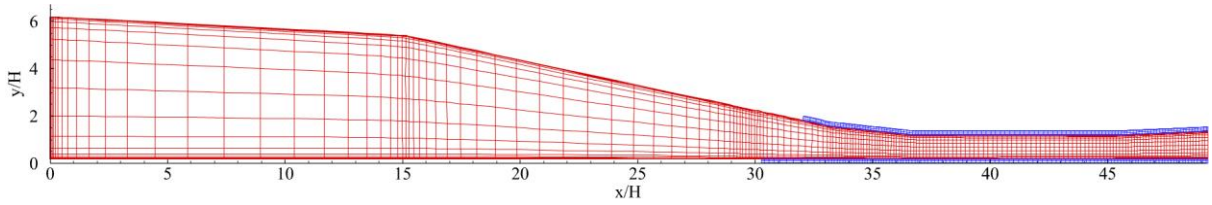

Fig 1. Computational domains and grid for CHT analysis (times 1/5)

3. Results

Figures 2 to 4 show the temperature contours for the adiabatic, constant wall temperature 150 K, and 300 K conditions. Under adiabatic conditions, the temperature of the flow field converged within 2 seconds. The interaction of the oblique shock with the boundary layer at x/H=35 and the change in the intensity of the oblique shock after x/H=43 were observed. The high temperature of the internal flow is not transferred to the structure by the insulated internal walls. As a result of the adiabatic conditions, it is unlikely that there will be any significant internal flow changes during the tens to hundreds of seconds of operation.

On the other hand, when the external wall temperature was given as a constant temperature, the internal flow field was visibly changing for tens of seconds. This change in flow field occurred faster than the temperature changes in the structure. For the structure, a sharp increase in solid temperature was observed at the cowl lip and corners. And it was also observed beyond the point of interaction with the reflected oblique shock from the cowl lip. This heating is caused by the increased stagnation temperature of the decelerated flow passing through the oblique shock. After 20 seconds, apart from the solid temperature on the upper wall, there were no noticeable differences in the internal flow patterns. The wall temperature was not heated above a certain level.

Figures 5-8 shows a graph of the temperature distribution of the near-wall flow at a specific moment. For the adiabatic condition, the temperature of the near-wall flow remains constant at all times without heat transfer. On the other hand, for CnsT 150 K to 300 K, the temperature gradually increases and converges to a similar temperature at 30 seconds. Although the temperature of each condition differs by 50 K, the physical properties and thickness of the structure are the same, so the temperature difference between each condition remains relatively even over time.

Density distribution graphs are shown in Figures 9-10 and pressure distribution graphs are shown in Figures 11-12 for 1 and 10 seconds of rapid temperature change. At 1 second, the density decreased by up to 7 times as the flow field near the wall heated up. At 10 seconds, the difference in density between the conditions decreased rapidly. The same trend was found for pressure, meaning that the magnitude of the density can still change during the time the structure is heated. It is important to note that density differences can also lead to differences in shock wave structure.

For CHTCT 150 K, which has the largest temperature gradient, the separation bubbles occurred at the front. This is due to the steepness of the boundary layer profile near the wall due to the low wall temperature, which caused the boundary layer to thicken. The thickening of the boundary layer pulls the location of the boundary layer-shock wave interaction forward. These differences can accumulate along the flow direction.

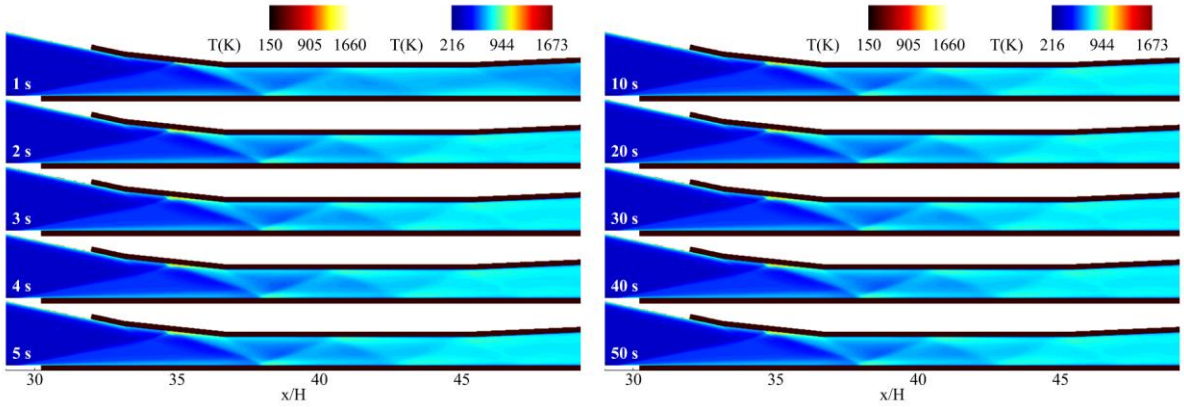

Fig 2. Temperature contour of the domains on the adiabatic wall condition

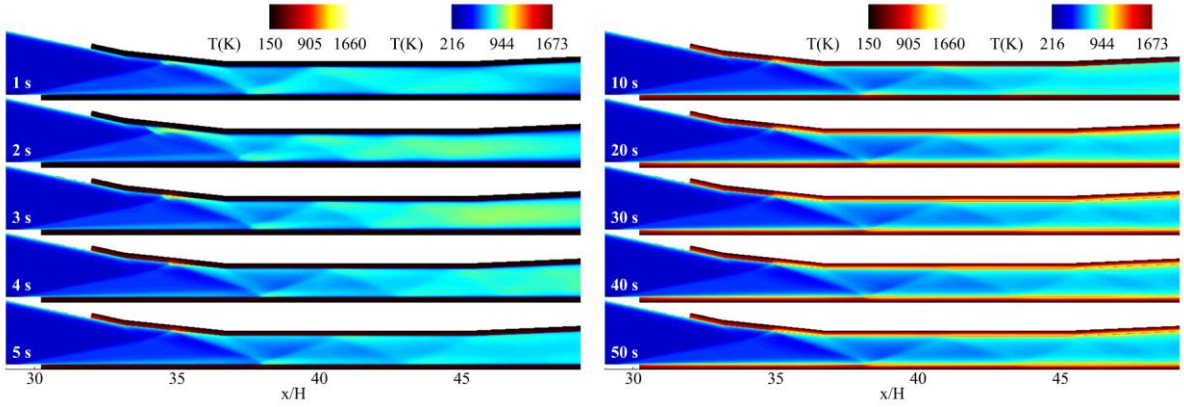

Fig 3. Temperature contour of the domains on the 150 K constant wall temperature condition

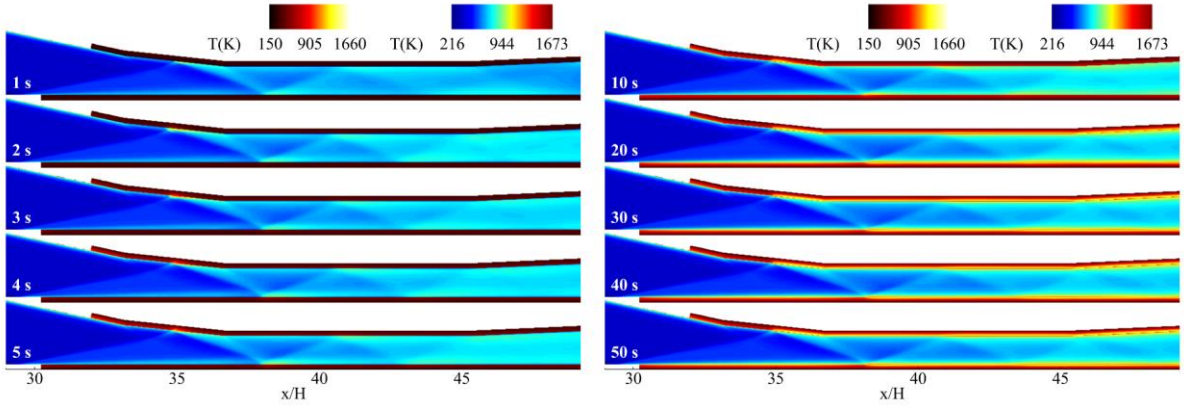

Fig 4. Temperature contour of the domains on the 300 K constant wall temperature condition

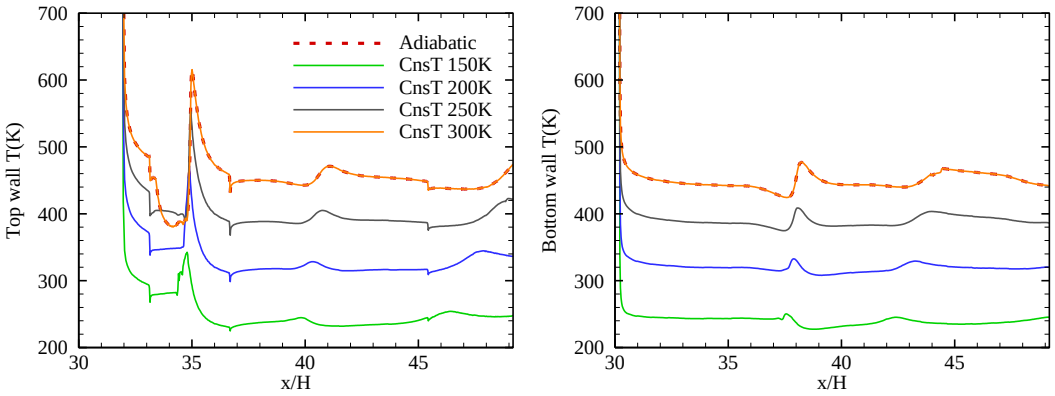

Fig 5. Temperature distribution with various conditions at 1 s (Left: top wall, Right: bottom wall)

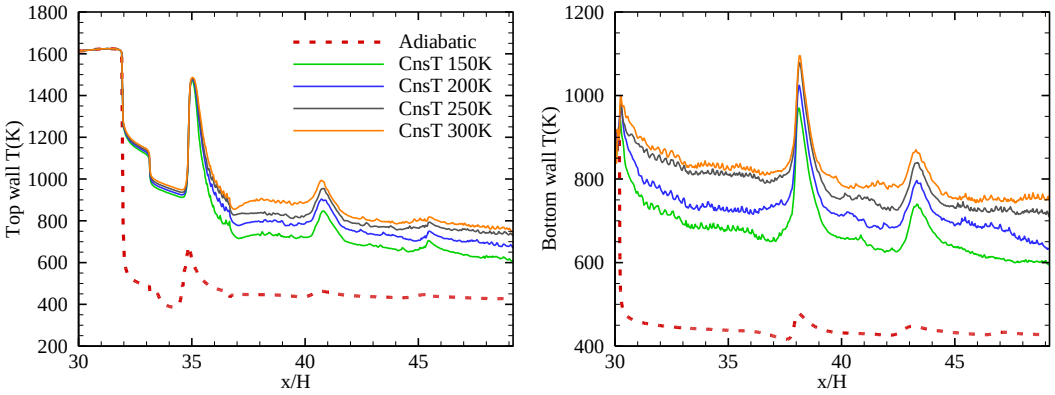

Fig 6. Temperature distribution with various conditions at 10 s (Left: top wall, Right: bottom wall)

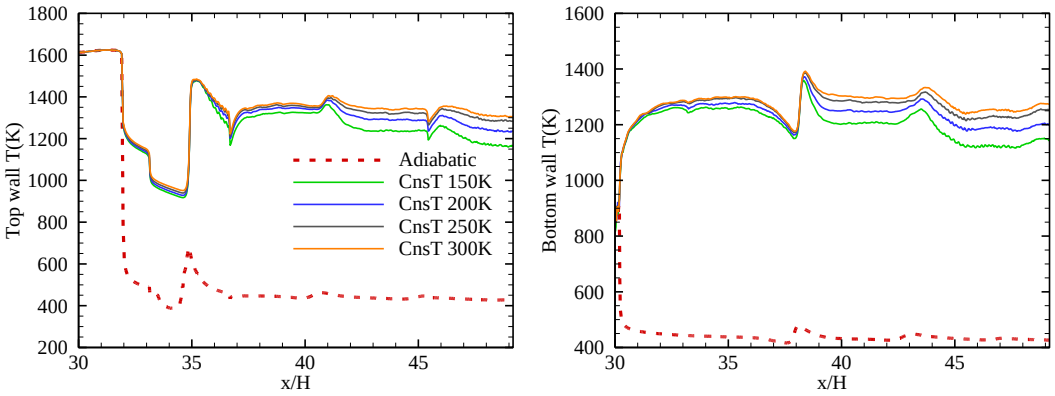

Fig 7. Temperature distribution with various conditions at 20 s (Left: top wall, Right: bottom wall)

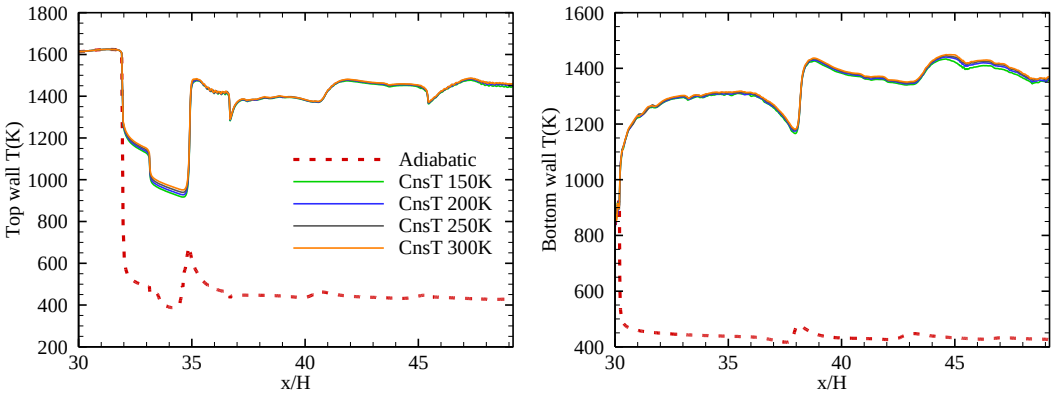

Fig 8. Temperature distribution with various conditions at 30 s (Left: top wall, Right: bottom wall)

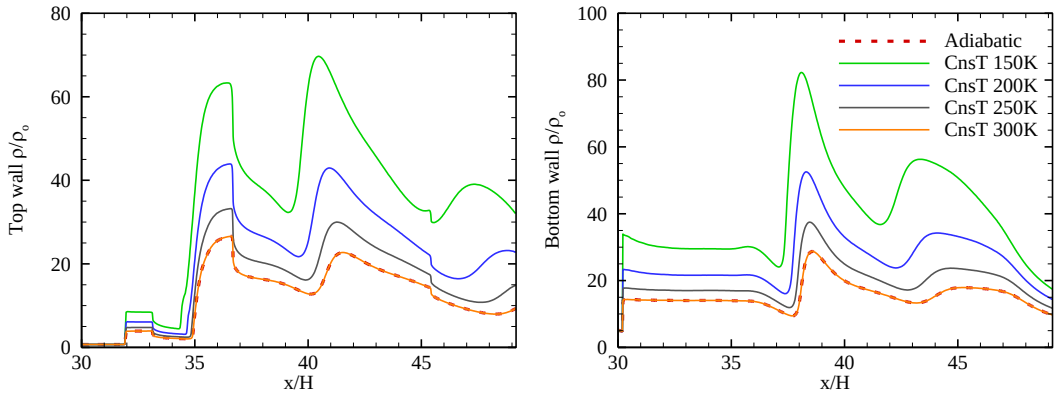

Fig 9. Density distribution with various conditions at 1 s (Left: top wall, Right: bottom wall)

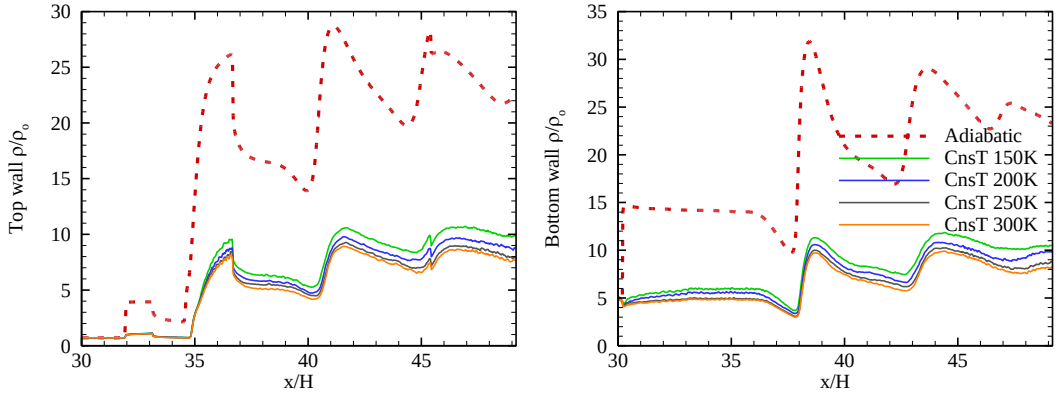

Fig 10. Density distribution with various conditions at 10 s (Left: top wall, Right: bottom wall)

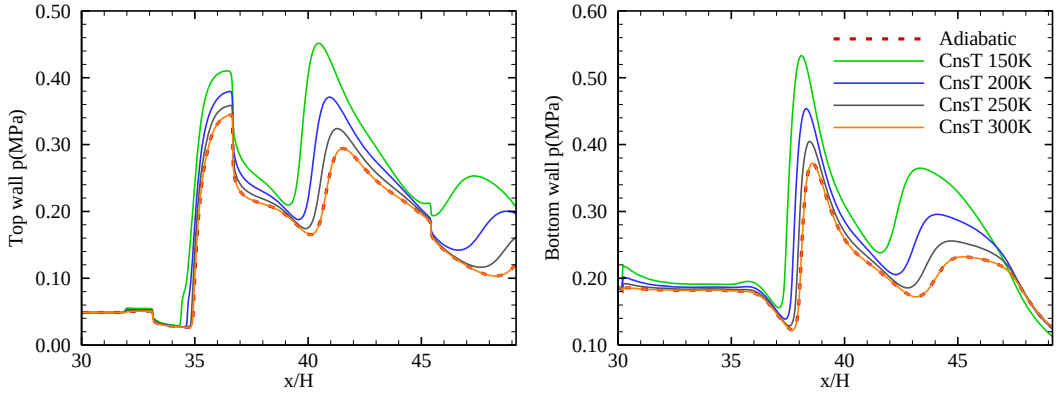

Fig 11. Pressure distribution with various conditions at 1 s (Left: top wall, Right: bottom wall)

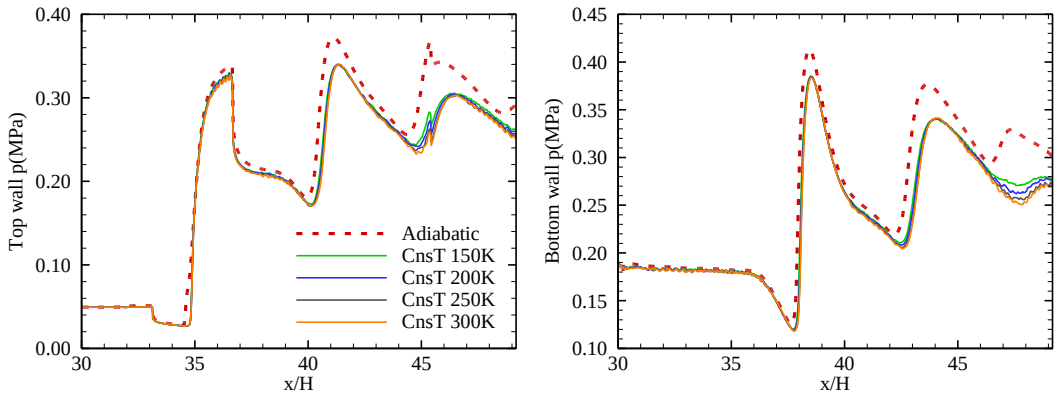

Fig 12. Pressure distribution with various conditions at 10 s (Left: top wall, Right: bottom wall)

4. Conclusion

A two dimensional CHT analysis was conducted to examine the internal flow field of the High-speed vehicle engine inlet. The temperature variations of the solid and fluid domains over time were observed, and the changes in the flow field due to boundary conditions were investigated.
Comparing the adiabatic wall boundary condition with the constant wall temperature conditions shows that the temperature of the structure affects the internal flow field. A low-temperature structure will transfer heat from a high-temperature fluid and heat up, which has the effect of cooling the fluid. Therefore, the temperature change in the fluid can persist before the temperature change in the structure converges. Changes in temperature lead to changes in density and pressure, which can also affect the oblique shock wave structure of the internal flow field and the location of the shock-boundary layer interaction(SBLI).
Test models that are directly connected to a VAH have their external walls exposed to the atmosphere, allowing the internal flow field to change over relatively long periods of time. On the other hand, a test model fully immersed in a high-speed wind tunnel has its external walls exposed to high-speed flow, so the internal flow field can converge in a relatively short period of time. When performing ground tests of a vehicle with a planned long flight profile, it is necessary to consider changes in the internal flow field due to heating of the structure.

Acknowledgments

This paper was supported by MOTIE(Ministry of Trade, Industry and Energy) and KEIT(Korea Evaluation Institute of Industrial Technology) in 2021 for the project of Development of oxide dispersion strengthened superalloy materials and manufacturing technology for hypersonic engines(1415176396, 20017647)

References

1. Choi, J.-Y., Ma, F., Yang, V.: Dynamics combustion characteristics in scramjet combustors with transverse fuel injection. 41st AIAA/ASME/SAE/ASEE Joint Propuls. Conf. and Exhib. (2005). https://doi.org/10.2514/6.2005-4428
2. Won, S.-H., Jeung, I.-S., Choi, J.-Y.: Turbulent combustion characteristics in HyShot model combustor with transverse fuel injection. 43rd AIAA/ASME/SAE/ASEE Joint Propuls. Conf. AIAA4124–4135 (2007). https://doi.org/10.2514/6.2007-5427
3. Jeong, S.-M., Choi, J.-Y.: Combined diagnostic analysis of dynamic combustion characteristics in a scramjet engine. Energ. 13(15), 4029 (2020). https://doi.org/10.3390/en13154029
4. Choi, J.-Y., Yang, V., Ma, F., Won, S.-H., Jeung, I.-S.: Detached Eddy simulation of combustion dynamics in scramjet combustors. Collection of Technical Papers - 43rd AIAA/ASME/SAE/ASEE Joint Propuls. Conf. 1, 231–237 (2007). https://doi.org/10.2514/6.2007-5027
5. Choi, J.-Y., Noh, J., Byun, J.-R., Lim, J. S., Togai, K., Yang, V.: Numerical investigation of combustion/shock-train interactions in a dual-mode scramjet engine. 17th AIAA Int. Space Planes and Hypersonic Syst. and Technol. Conf. 2011 (2011). https://doi.org/10.2514/6.2011-2395
6. Noh, J., Choi, J.-Y., Yang, V.: Numerical Simulation of Ethylene Fueled Scramjet Combustor with Air Throttling. Part 1: Auto-Ignition. J. of Propuls. and Energy 1(1), 32-43 (2020). https://doi.org/10.6108/JPNE.2020.1.1.032
7. Choi, J.-Y., Noh, J., Jeong, S. M., Kim, J. E., Yang, V.: Numerical Simulation of Ethylene Fueled Scramjet Combustor with Air Throttling, Part2: Transient Details. J. of Propuls. and Energ. 2(1), 44-58 (2021). https://doi.org/10.6108/JPNE.2021.2.1.044
8. Choi, J.-Y., Unnikrishnan, U., Hwang, W.-S., Jeong, S.-M., Han, S.-H., Kim, K. H, Yang, V.: Effect of fuel temperature on flame characteristics of supersonic turbulent combustion. Fuel 329, 125310 (2022). https://doi.org/10.1016/j.fuel.2022.125310

9. Kim, H.-S., Oh, S., Choi, J.-Y.: Quasi-1D analysis and performance estimation of a sub-scale RBCC engine with chemical equilibrium. Aerosp. Sci. and Technol. 69, 39–47 (2017). https://doi.org/10.1016/j.ast.2017.06.019
10. Kim, H.-S., Kim, K.-S., Oh, S.-J., Choi, J.-Y., Yang, W.-S.: A preliminary design of flight test conditions for a sub-scale RBCC engine using a sounding rocket. Int. J. of Aeronaut. and Space Sci. 16(4), 529–536 (2015). https://doi.org/10.5139/IJASS.2015.16.4.529
11. Vyasaprasath, K., Oh, S., Kim, K.-S., Choi, J.-Y.: Numerical studies of supersonic planar mixing and turbulent combustion using a detached eddy simulation (DES) model. Int. J. of Aeronaut. and Space Sci. 16(4), 560–570 (2015). https://doi.org/10.5139/IJASS.2015.16.4.560
12. Won, S.-H., Jeung, I.-S., Shin, J.-R., Cho, D.-R., Choi, J.-Y.: Three-dimensional dynamic characteristics of transverse fuel injection into a supersonic cross flow. 15th AIAA Int. Space Planes and Hypersonic Syst. and Technol. Conf. 2008-2515 (2008). https://doi.org/10.2514/6.2008-2515
13. Jeong, S.-M., Lee, J.-H., Choi, J.-Y.: Numerical investigation of low-frequency instability and frequency shifting in a scramjet combustor. Proc. of the Combust. Inst. 39(3), 3107–3116 (2023). https://doi.org/10.1016/j.proci.2022.07.245
14. Jeong, S.-M., Han, H.-S., Sung, B.-K., Kim, W., Choi, J.-Y.: Reactive Flow Dynamics of Low-Frequency Instability in a Scramjet Combustor. Aerosp. 10(11), 932 (2023). https://doi.org/10.3390/aerospace10110932
15. Lee, J.-H., Lee, E.-S., Han, H.-S., Kim, M.-S., Choi, J.-Y.: A Study on a Vitiated Air Heater for a Direct-Connect Scramjet Combustor and Preliminary Test on the Scramjet Combustor Ignition. Aerosp. 10(5), 415 (2023). https://doi.org/10.3390/aerospace10050415
16. Sung, B.-K., Jeong, S.-M., Choi, J.-Y.: Direct-connect supersonic nozzle design considering the effect of combustion. Aerosp. Sci. and Technol. 133, 108094 (2023). https://doi.org/10.1016/j.ast.2022.108094
17. Sung, B.-K., Hwang, W.-S., Choi, J.-Y.: Design of a Shape Transition Nozzle for Lab-scale Supersonic Combustion Experimental Equipment. J. of the Korean Soc. for Aeronaut. and Space Sci. 48(3), 207–215 (2020). https://doi.org/10.5139/JKSAS.2020.48.3.207
18. Lee, E.-S., Han, H.-S., Lee J.-H., Choi, J.-Y.: A Study on the Flow Conditions of the Combustion Air Heater Outlet for the Supersonic Combustion Experiment. J. of the Korean Soc. of Propuls. Eng. 26(1) 88097, (2022). https://doi.org/10.6108/KSPE.2022.26.1.088
19. Kim, M.-S., Koo, I.-H., Lee, K.-H., Lee, E.-S., Han, H.-S., Jeong, S.-M., Kim, H., Choi, J.-Y.: Experimental Study on the Ignition Characteristics of Scramjet Combustor with Tandem Cavities Using Micro-Pulse Detonation Engine. Aerosp. 10(8), 706 (2023). https://doi.org/10.3390/aerospace10080706
20. Choi, J.-Y., Han, S.-H., Kim, K.H., Yang, V.: High resolution numerical study on the coaxial supersonic turbulent flame structures. 50th AIAA/ASME/SAE/ASEE Joint Propuls. Conf. 2014, (2014). https://doi.org/10.2514/6.2014-3745
21. Kim, S.D., Lee, B.J., Lee, H.J. Jeung, I.-S., Choi, J.-Y.: Realization of contact resolving approximate Riemann solvers for strong shock and expansion flows. Int. J. Num. Methods in Fluids 62(10), 1107–1133 (2020). https://doi.org/10.1002/fld.2057
22. Kim, S.-L., Choi, J.-Y., Jeung, I.-S., Park, Y.-H.: Application of approximate chemical Jacobians for constant volume reaction and shock-induced combustion. Applied Numer. Math. 39(1), 87–104 (2001). https://doi.org/10.1016/S0168-9274(01)00054-X
23. Kim, S.-L., Jeung, I.-S., Choi, J.-Y., Park, Y.-H.: Approximate Jacobian methods for efficient calculation of reactive flows. 36th AIAA/ASME/SAE/ASEE Joint Propuls. Conf. and Exhib. (2000). https://doi.org/10.2514/6.2000-3384

24. Kumar, P.P., Kim, K.-S., Oh, S., Choi, J.-Y.: Numerical comparison of hydrogen-air reaction mechanisms for unsteady shock-induced combustion applications. J. of Mechanical Sci. and Technol. 29(3), 893–898 (2015). https://doi.org/10.1007/s12206-015-0202-2
25. Choi J.-Y., Jeung I.-S., Yoon Y.: Computational fluid dynamics algorithms for unsteady shock-induced combustion. Part 1: validation. AIAA J. 38(7), 1179-1187 (2000). https://doi.org/10.2514/2.1112
26. Choi J.-Y., Jeungt I.-S., Yoon Y.: Computational fluid dynamics algorithms for unsteady shock-induced combustion. Part 2: comparison. AIAA J. 38(7), 1188-1195 (2000). https://doi.org/10.2514/2.1087
27. Choi, J.-Y., Jeung, I.-S., Yoon, Y.: Validation of CFD algorithms for unsteady shock-induced combustion. 34th AIAA/ASME/SAE/ASEE Joint Propuls. Conf. and Exhib. A98-3217, (1998). https://doi.org/10.2514/6.1998-3217
28. Choi J.-Y., Shin E.J.-R., Jeung I.-S.: Unstable combustion induced by oblique shock waves at the non-attaching condition of the oblique detonation wave. Proc. Combust. Inst. 32(II), 2387-2396 (2009). https://doi.org/10.1016/j.proci.2008.06.212
29. Choi J.-Y., Jeung I.-S., Yoon Y.: Numerical study of scram accelerator starting characteristics. AIAA J. 36(6), 1029-1038 (1998). https://doi.org/10.2514/2.476
30. Choi, J.-Y., Jeung, I.-S., Yoon, Y.: Unsteady-state simulation of model ram accelerator in expansion tube. AIAA J. 37(5), 537–543 (1999). https://doi.org/10.2514/2.770
31. Choi, J.-Y., Jeung, I.-S., Yoon, Y.: Scaling effect of the combustion induced by shock-wave boundary-layer interaction in premixed gas. Symp. (Int.) on Combust. 27(2), 2181–2188 (1998). https://doi.org/10.1016/S0082-0784(98)80067-2
32. Choi, J.-Y., Jeung, I.-S., Lee, S.: Dimensional analysis of the effect of flow conditions on shock-induced combustion. Symp. (Int.) on Combust. 26(2), 2925–2932 (1996). https://doi.org/10.1016/S0082-0784(96)80134-2
33. Pavalavanni, P.K., Sohn, C.H., Lee, B.J., Choi, J.-Y.: Revisiting unsteady shock-induced combustion with modern analysis techniques, Proc. of the Combust. Inst. 37(3), 3637–3644 (2019). https://doi.org/10.1016/j.proci.2018.07.094
34. Choi, J.-Y., Jeung, I.-S., Yoon, Y.: Transient simulation of superdetonative mode initiation process in scram-accelerator, Symp. (Int.) on Combust. 26(2), 2957–2963 (1996). https://doi.org/10.1016/S0082-0784(96)80138-X
35. Choi, J.-Y., Shin, E.J.-R., Cho, D.-R., Jeung, I.-S., Yang, V.: Onset condition of oblique detonation wave cell structures, 46th AIAA Aerosp. Sci. Meeting and Exhib. 2008-1032 (2008). https://doi.org/10.2514/6.2008-1032
36. Pavalavanni, P.K., Jo, M.-S., Kim, J.-E., Choi, J.-Y.: Numerical Study of Unstable Shock-Induced Combustion with Different Chemical Kinetics and Investigation of the Instability Using Modal Decomposition Technique. Aerosp. 10(3), 292 (2023). https://doi.org/10.3390/aerospace10030292
37. Menter, F.R.: Two-Equation Eddy-Viscosity Turbulence Models for Engineering Applications. AIAA J. 32, 1598-1605 (1994). https://doi.org/10.2514/3.12149
38. Won, S.-H., Jeung, I.-S., Choi, J.-Y.: DES study of transverse jet injection into supersonic cross Flows. 44th AIAA Aerosp. Sci. Meeting 20, 14908–14915 (2006). https://doi.org/10.2514/6.2006-1227
39. Won, S.-H., Jeung, I.-S., Choi, J.-Y.: DES investigation of the ignition of hydrogen transverse jet into high enthalpy supersonic crossflow. 47th AIAA Aerosp. Sci. Meeting including the New Horizons Forum and Aerosp. Expo. 2009-1557 (2009). https://doi.org/10.2514/6.2009-1557

40. Choi, J.-Y., Yang, V., Fuhua, M., Won, S.-H., Jeung, I.-S.: DES Modeling of Supersonic Combustion in Scramjet Combustors. AIAA/ASME/SAE/ASEE 42nd Joint Propuls. Conf. 9 (2006). https://doi.org/10.2514/6.2006-5097
41. Choi, J.-Y., Shin, E., Kim, C.-K.: Numerical study of base-bleed projectile with external combustion. 41st AIAA/ASME/SAE/ASEE Joint Propuls. Conf. and Exhib. (2005). https://doi.org/10.2514/6.2005-4352
42. Shin, J.-R., Cho, D.-R., Won, S.-H., Choi, J.-Y.: Hybrid RANS/LES study of base-bleed flows in supersonic mainstream. 15th AIAA Int. Space Planes and Hypersonic Syst. and Technol. Conf. 2008-2588 (2008). https://doi.org/10.2514/6.2008-2588
43. Shin, J.-R., Choi, J.-Y.: Dynamic Correction of DES Model Constant for the Advanced Prediction of Supersonic Base Flow. J. of the Korean Soc. for Aeronaut. and Space Sci. 38(2), 99-110 (2010). https://doi.org/10.5139/JKSAS.2010.38.2.099
44. Chakravarthy, S., Osher, S.: High Resolution Applications of the Osher Upwind Scheme for the Euler Equations. 6th Comput. Fluid Dyn. Conf. Danvers 1943 (1983). https://doi.org/10.2514/6.1983-1943
45. Shuen, J.S., Yoon, S.: Numerical Study of Chemically Reacting Flows Using a Lower-Upper Symmetric Successive Overrelaxation Scheme. AIAA J. 27, 1752-1760 (1989). https://doi.org/10.2514/3.10331
46. Wieting, A.R.: Experimental Study of Shock Wave Interference Heating on Cylindrical Leading Edge. NASA TM-100484 (1987)
47. Kim, J.-E., Choi, J.-Y.: Numerical Analysis of Scramjet Inlet and Isolator According to the Heat Transfer Boundary Condition. Proc. of the the 34th Int. Symp. On Shock Waves, Daegu, Korea (2023)
48. Kim, J.-E., Jeong, S.-M., Kim, W.D., Choi, J.-Y., Hwang, Y.: Numerical analysis of internal flow thermal environment in an accelerating high–speed vehicle. Aerosp. Sci. and Technol. 145, 108889 (2024). https://doi.org/10.1016/j.ast.2024.108889